(Axisymmetric) Disruption Modeling with NIMROD

C. R. Sovinec and K. J. Bunkers

University of Wisconsin-Madison

Meeting of the Center for Extended MHD

March 15, 2015

Courant Institute, New York University

Objective

Our aim is to show initial results with representative profiles and with different boundary conditions on flow velocity and particle flux.

Outline

- Introduction
- Modeling with NIMROD
    - Initialization
    - MHD system and boundary conditions
- Axisymmetric results
    - Physical conditions
    - Results
- Discussion and conclusions

Introduction: Simulations of VDEs can be used to predict their effects in future devices.

- VDEs have greater potential for causing physical damage than other ‘off-normal’ events.
- The goal of nonlinear extended-MHD VDE simulations is to quantify predictions.
    - Assess heat and mechanical stresses.
    - Predict onset of 3D instability and its effects.
    - For example, see Strauss, Paccagnella, and Breslau, PoP **17**, 82505 (2010).
- Besides core MHD, simulations need resistive wall and external-mode capabilities.

Modeling with NIMROD: Disruption simulation requires attention to initialization, boundary conditions, and coupling to external regions.

For initialization, we have enhanced the NIMEQ solver [Howell and Sovinec, CPC **185**, 1415] to distinguish open- and closed-flux regions without aligned meshing.

- Using $\mathbf{B}_{pol}$ *only*, field-lines are traced from NIMROD's spectral-element nodes during each Picard iteration.
- Traces reaching a modest upper limit before hitting the domain boundary identify points within the closed flux.
- The identification is used when evaluating $P(\psi)$ and $F(\psi)$.
- Fields from external coils are included, but our Grad-Shafranov computations are fixed-boundary at this point.

An example shows the initialization for one of the cases presented later.

- Expecting large n=0 displacement, the mesh is rectangular (72×96, bicubic) and not aligned with the magnetic flux.
- The stopping length for poloidal-field tracing is $6\times R_{outer}$.

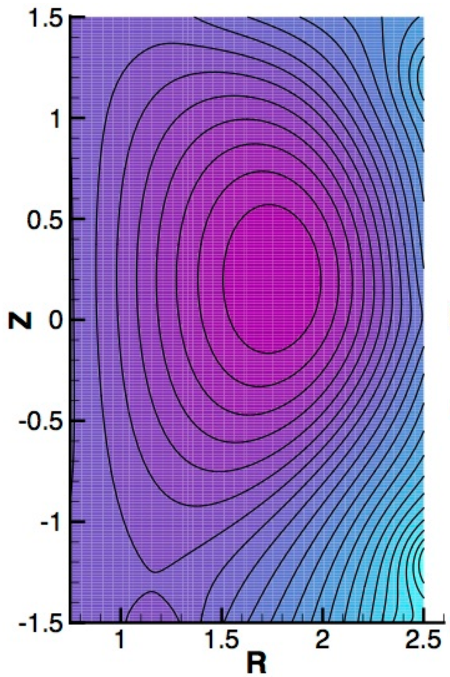

Final ψ distribution has one *X*-point inside the domain.

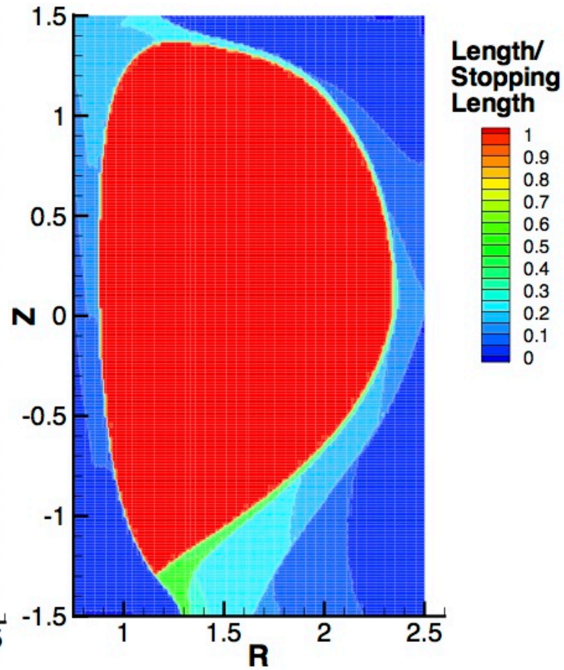

Normalized length as a function of launch point identifies closed flux.

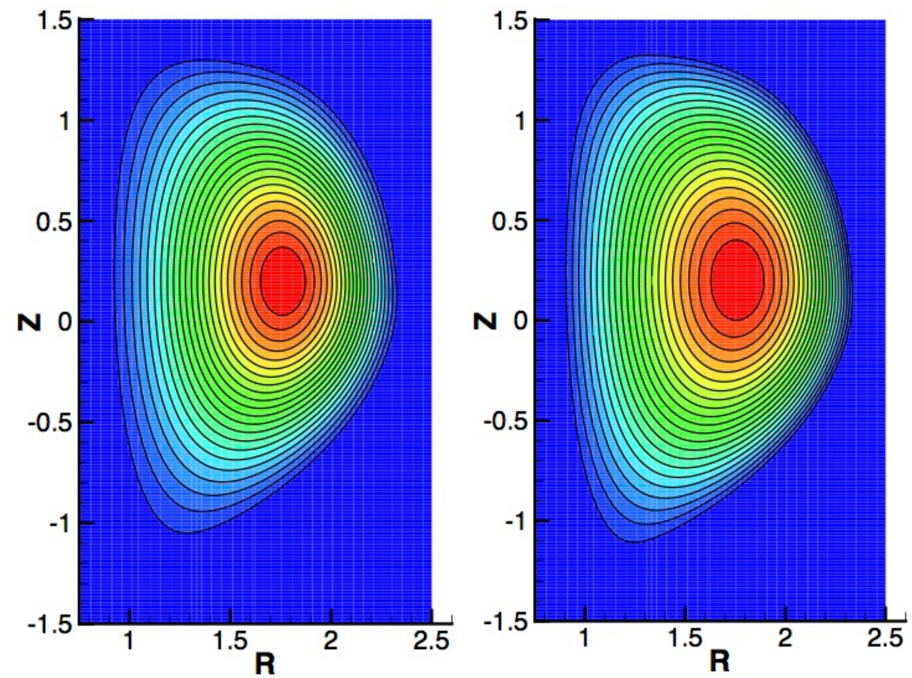

Pressure (left) and $F=RB_\phi$ (right) are prescribed to be constant where the normalized length is less than unity.

Plasma evolution from the initial state is modeled with NIMROD's single-fluid, single-temperature system.

$$\frac{\partial n}{\partial t} + \nabla \cdot (n\mathbf{V}) = \nabla \cdot \left(D_n \nabla n - D_h \nabla \nabla^2 n \right)$$

continuity with diffusive numerical fluxes

$$mn\left(\frac{\partial}{\partial t} + \mathbf{V} \cdot \nabla \right)\mathbf{V} = \mathbf{J} \times \mathbf{B} - 2\nabla (nT) - \nabla \cdot \underline{\Pi}$$

flow evolution

$$\frac{3}{2} n\left(\frac{\partial}{\partial t} + \mathbf{V} \cdot \nabla \right)T = -nT\nabla \cdot \mathbf{V} - \nabla \cdot \mathbf{q}$$

temperature evolution

$$\frac{\partial \mathbf{B}}{\partial t} = -\nabla \times (\eta \mathbf{J} - \mathbf{V} \times \mathbf{B}) + \kappa_b \nabla \nabla \cdot \mathbf{B}$$

Faraday's / Ohm's law with diffusive error control

$$\mu_0 \mathbf{J} = \nabla \times \mathbf{B}$$

low-ω Ampere's law

- The diffusive control of divergence error works well with high-order elements [Sovinec, *et al*., JCP **195**, 355 (2004)].
- The particle diffusion terms provide numerical smoothing.
- Two-fluid modeling will be applied in subsequent disruption studies.

The present modeling is simplified, but closure relations and diffusivity parameters are important.

- Spitzer $\eta \sim T^{-3/2}$ is used throughout the central computational region that models plasma.
  - The cases shown below have $\tau_A \cong 1$ and $\eta(0)=10^{-6}$. With $a \cong 0.75$, $S(0) \cong 5\times10^{5}$. T profiles vary by 10^{4}, but η is limited to 10^{-2} in most cases.
  - Number density profiles vary by 10.
- Thermal conduction is anisotropic, $\mathbf{q} = -n\left[\chi_{\|}\hat{\mathbf{b}}\hat{\mathbf{b}} + \chi_{\perp}\left(\mathbf{I}-\hat{\mathbf{b}}\hat{\mathbf{b}}\right)\right]\cdot\nabla T$, with $\chi_{\|}=5\times10^{-2}$ and $\chi_{\perp}=5\times10^{-6}$.
- Viscous stress is isotropic, $\underline{\Pi} = -nm_i\nu_{iso}\left(\nabla\mathbf{V}+\nabla\mathbf{V}^{\mathrm{T}}-\frac{2}{3}\underline{\mathbf{I}}\nabla\cdot\mathbf{V}\right)$, with $\nu_{iso}=5\times10^{-5}$.
- The artificial particle diffusivities are set to $D_n=5\times10^{-6}$ and $D_h=1\times10^{-10}$.

The plasma region is coupled to an external vacuum through a resistive wall.

- Plasma modeling is in the central region only.
- The central region is coupled to a meshed external region that is also solved in NIMROD's representation.
- The plot on the right demonstrates poloidal flux leaking into a horseshoe-shaped external region (used in the following).
- Regions are coupled by an implicit implementation of the thin-wall equation.

$$\frac{\partial \mathbf{B}\cdot\hat{\mathbf{n}}}{\partial t} = -\hat{\mathbf{n}}\cdot\nabla\times\left[\left(\frac{\eta_w}{\mu_0 \delta x}\right)\hat{\mathbf{n}}\times\delta\mathbf{B}\right]$$

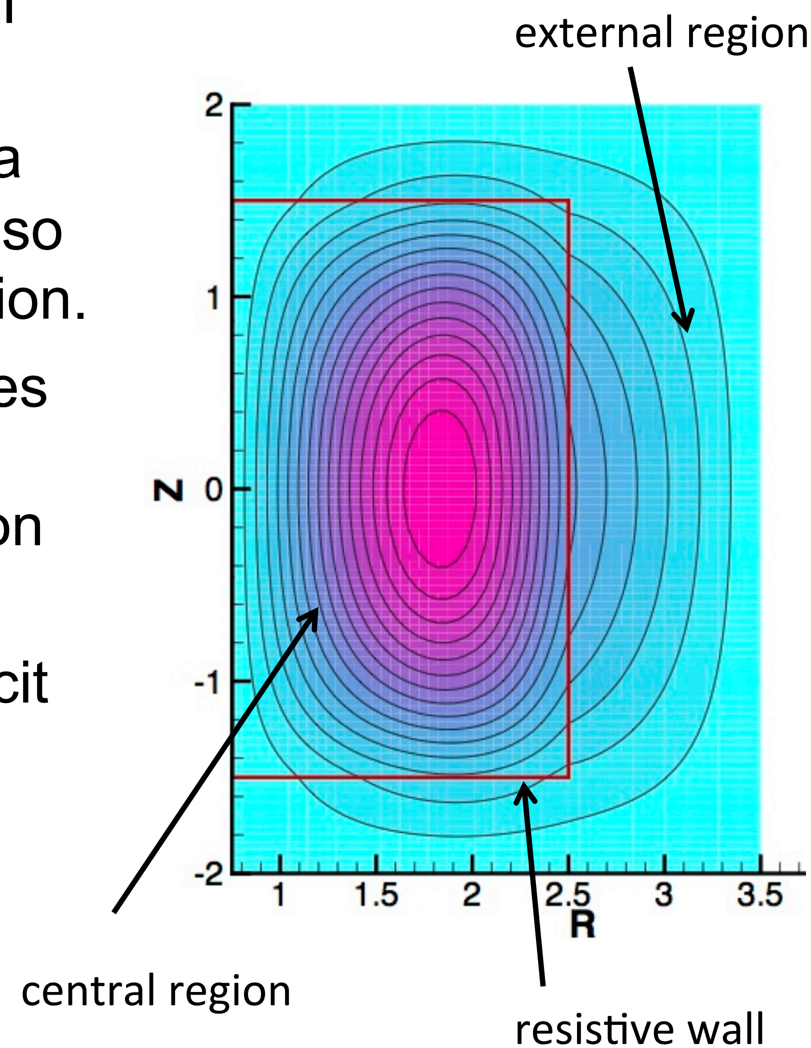

Boundary conditions on **B** are set at the outer boundary, while conditions on *n*, *T*, and **V** are set along the perimeter of the central region.

- Standard conditions for NIMROD simulations with thermal conduction and particle diffusion are:
  - *n* and *T* remain fixed at their initial low values.
  - All components of flow are zero, **V** = 0. *"Salt water"*
- Conditions based on magnetic drift have been implemented:
  - Flow drifts out, based on the resistive-wall **E**. *"DEBS"*

    $$\hat{\mathbf{n}}\cdot\mathbf{V}=\hat{\mathbf{n}}\cdot\frac{1}{B^2}\mathbf{E}_w\times\mathbf{B}\ \text{, where } \mathbf{E}_w=\left(\frac{\eta_w}{\mu_0\delta x}\right)\hat{\mathbf{n}}\times\delta\mathbf{B}$$
  - *T* remains fixed at its initial value.
  - *n* is either fixed *or* advects into the resistive wall, $\hat{\mathbf{n}}\cdot\Gamma=\hat{\mathbf{n}}\cdot\left(n\mathbf{V}\right)$, which has been implemented with the explicit (old) *n* at each step.
- Along the outer boundary, $\hat{\mathbf{n}}\times\mathbf{E}=\mathbf{0}$, so $\hat{\mathbf{n}}\cdot\mathbf{B}$ is fixed.

Development for parallel communication across (resistive-wall) interfaces is near completion.

- The NIMROD strategy considers each region as a separate domain that is coupled to other domains.
- Domain decomposition is applied to each region with the same set of processes.
- The geometry of the interface and the decompositions of the regions dictate communication patterns.
- In the example shown at right, process 1 communicates with 0 and 2, while processes 0 and 2 only communicate with process 1.
- Parallel computations reproduce single-process results on small test cases but not for others. Results shown here have been produced with serial computations.

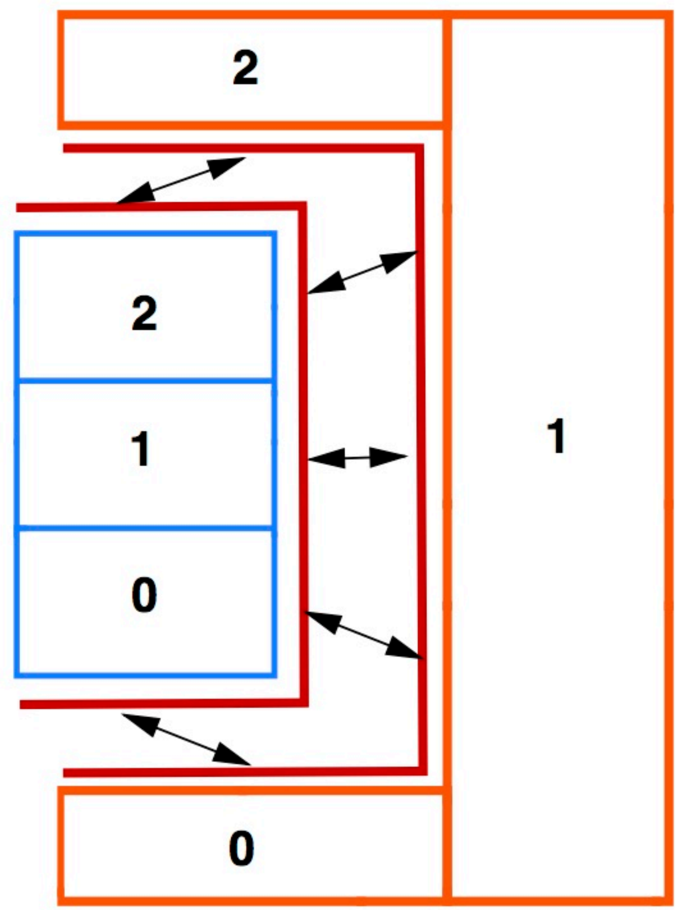

Schematic shows a 2-region, 3-process example. Each region has subdomains, and processes are numbered from 0.

Axisymmetric results: Recent computations demonstrate progress for VDE tokamak simulation.

- The aspect ratio and elongation are representative.
- $P(\psi)$ and $F(\psi)$ profiles are simple quadratic and linear functions, respectively, but values are based on DIII-D with F nearly uniform and $\beta(0)$=8%.
- There is no applied loop voltage in these computations, so current is free to decay.
  - τ_r for the initial profile is of order 10^5.
  - With $\eta_w/\mu_0\delta x = 10^{-3}$ and $a \sim 1$, $\tau_w \sim 10^3$.
  - The resistive wall sets the time-scale for evolution.
- Equilibria are computed with wall eddy currents, in addition to fixed external coil currents, and decay of the initial eddy currents leads to axisymmetric instability.

A “control” case with conducting walls around the central region shows slight evolution over 400 τ_A.

- Plasma current decreases by 4.3%.
- Thermal energy decreases by 1.5%

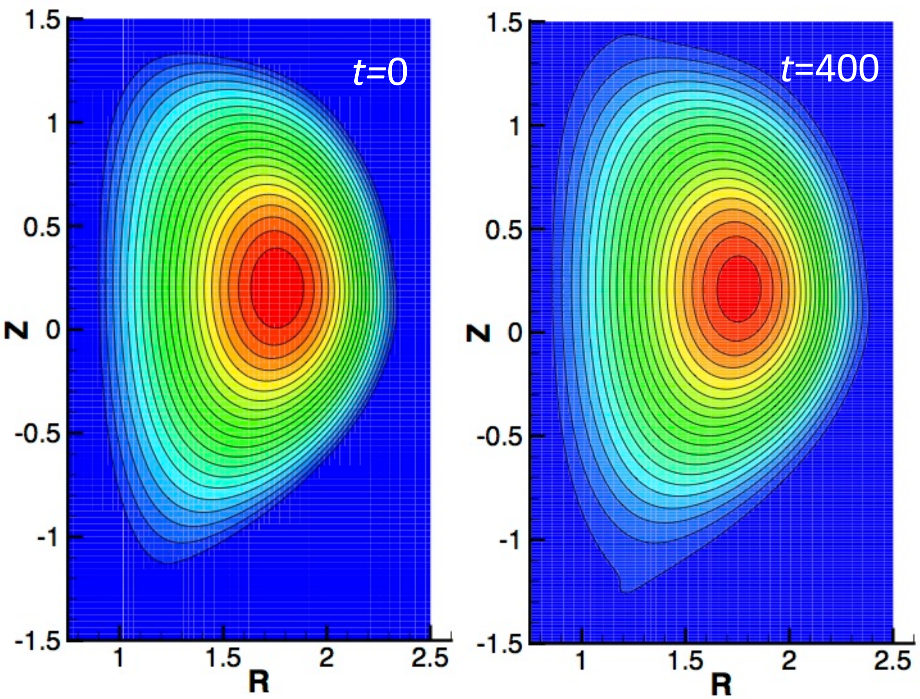

Comparison of initial and final *T* profiles indicates slight spreading near separatrix.
Note: color is not rescaled in these figures.

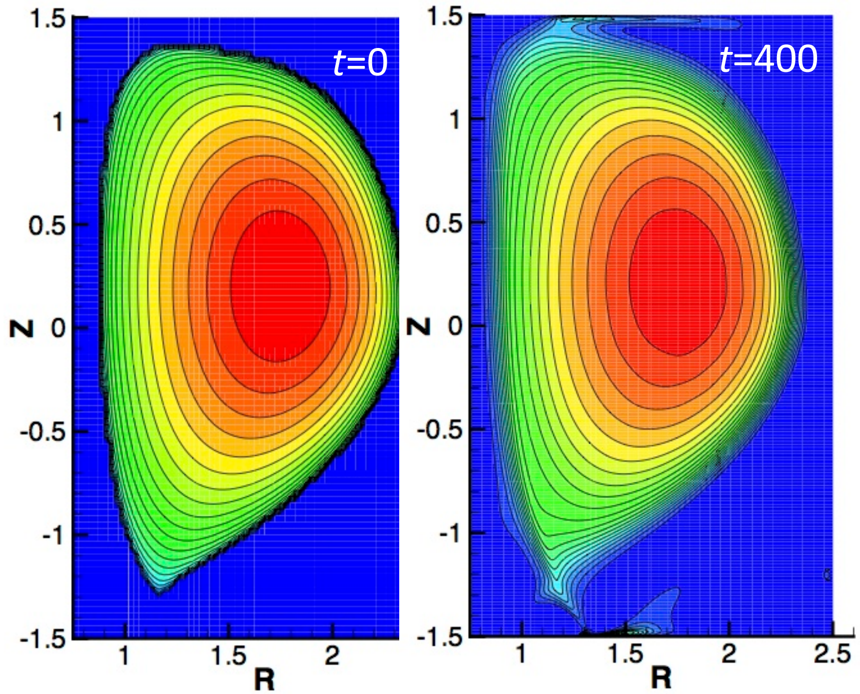

Comparison of initial and final *n* profiles shows weak diffusion and some leakage.

With a resistive wall, decay of eddy currents leads to slow axisymmetric instability.

- Over ~1000 τ_A, plasma current (I_p) decreases by 50% and thermal energy decreases by 85%.

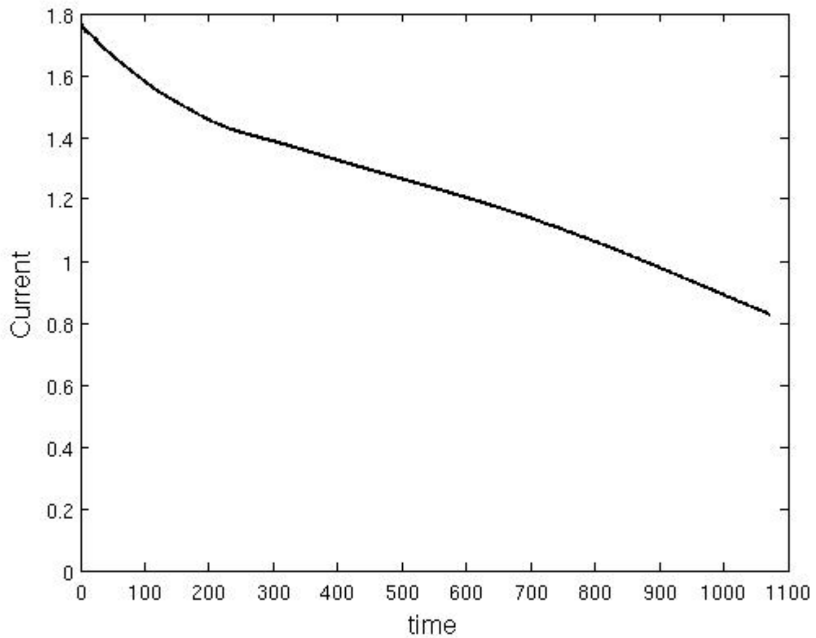

Plasma current evolution through 1000 τ_A.

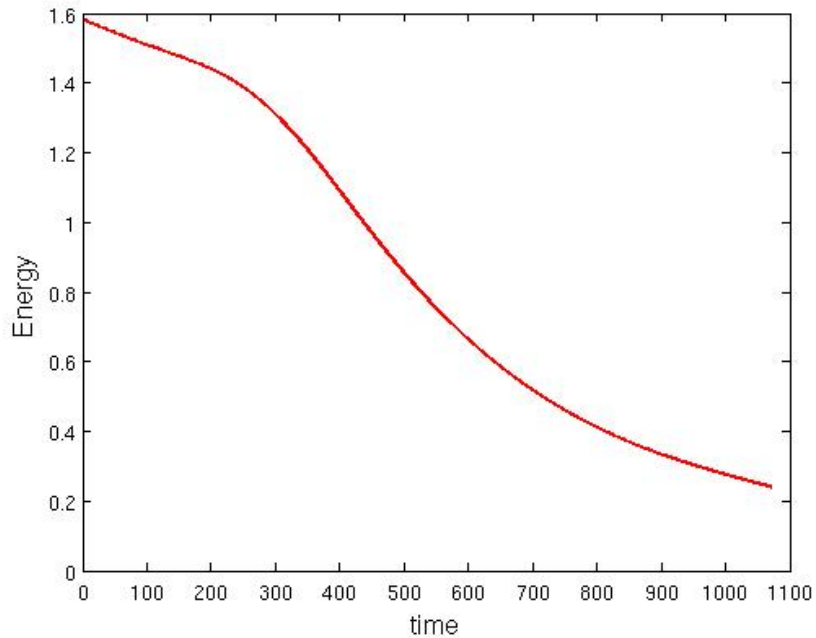

Internal energy decays faster than current after 300 τ_A due to thermal transport from outer surfaces.

- In these cases, the external coils stabilize the displacement after the wall eddy currents dissipate, and a small limited tokamak remains.

Displacement from the decay of eddy currents is primarily radial in these cases.

- This configuration has an attracting coil at R=2.6, Z=0 (triangularity) between vertical-field coils at Z=±1.2.
- Edge plasma cools through contact with the wall.

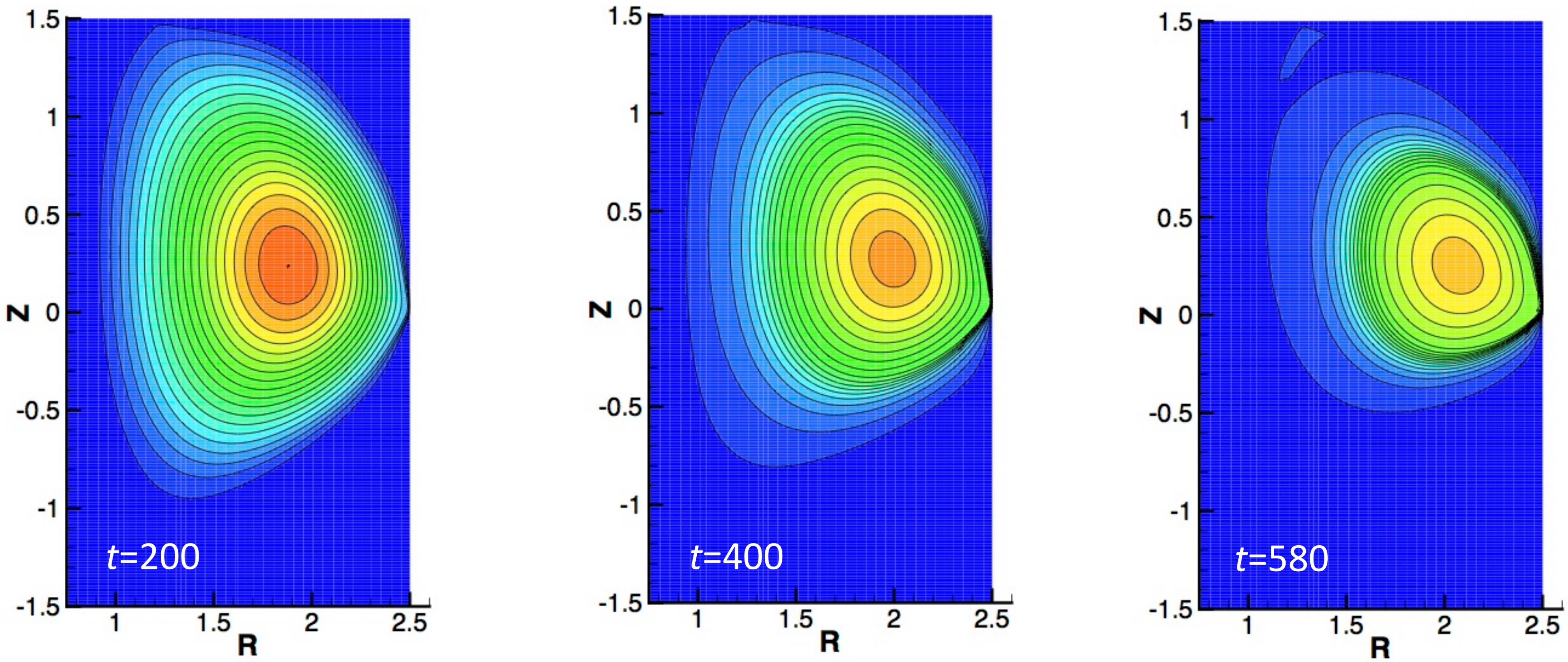

- Note that the evolution is significant relative to the control case.

With the Dirichlet boundary condition on *n*, diffusion allows mass to escape.

- Mass piles-up in layers near the points of contact.
- Outward mass flux results from $\hat{\mathbf{n}} \cdot \boldsymbol{\Gamma}_D = -\hat{\mathbf{n}} \cdot D_n \nabla n$ along the surface.

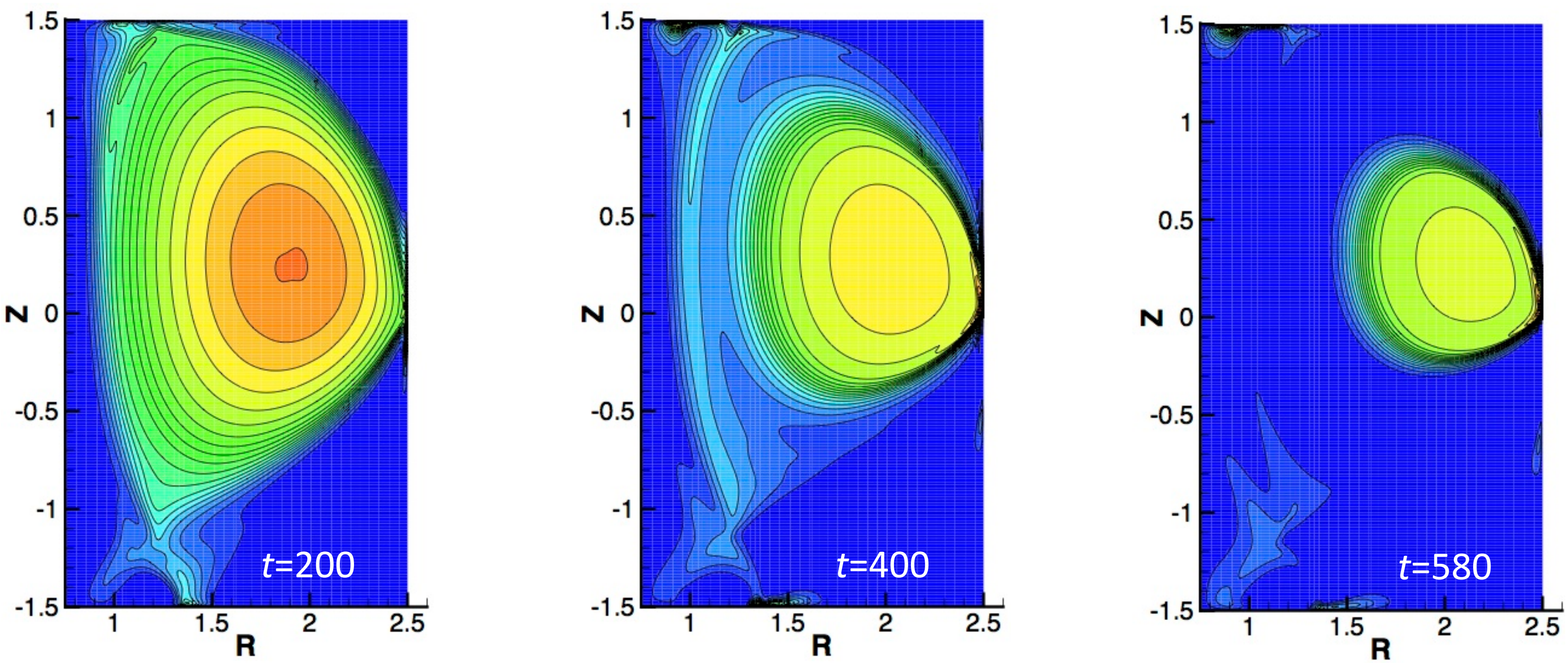

The evolution of current and thermal energy is essentially unchanged when the normal component of flow is set by $\mathbf{E}_w \times \mathbf{B}$ drift.

- The comparison is presently available through 300 τ_A.
- In this case, mass flow through the boundary is set by $\hat{\mathbf{n}} \cdot \Gamma = \hat{\mathbf{n}} \cdot \left(n\mathbf{V}\right)$.

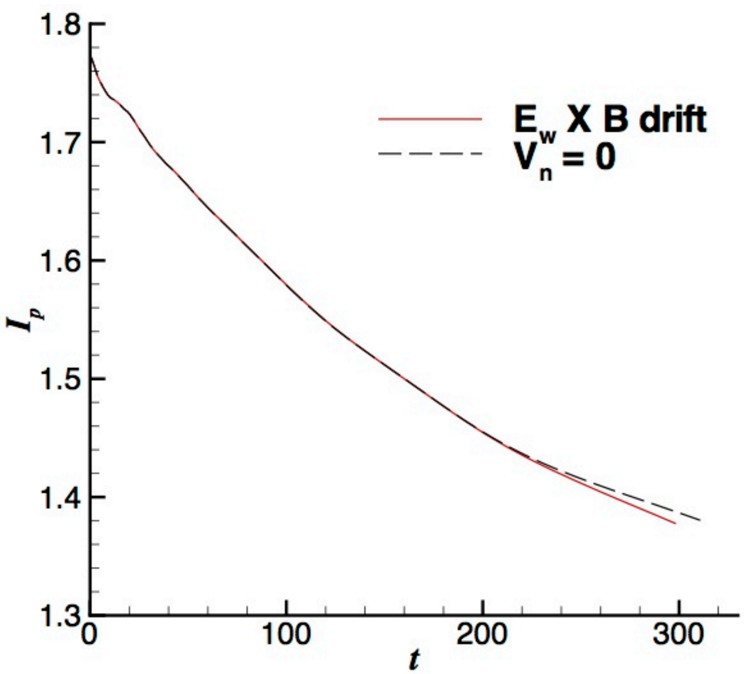

Plasma current comparison through 300 τ_A.

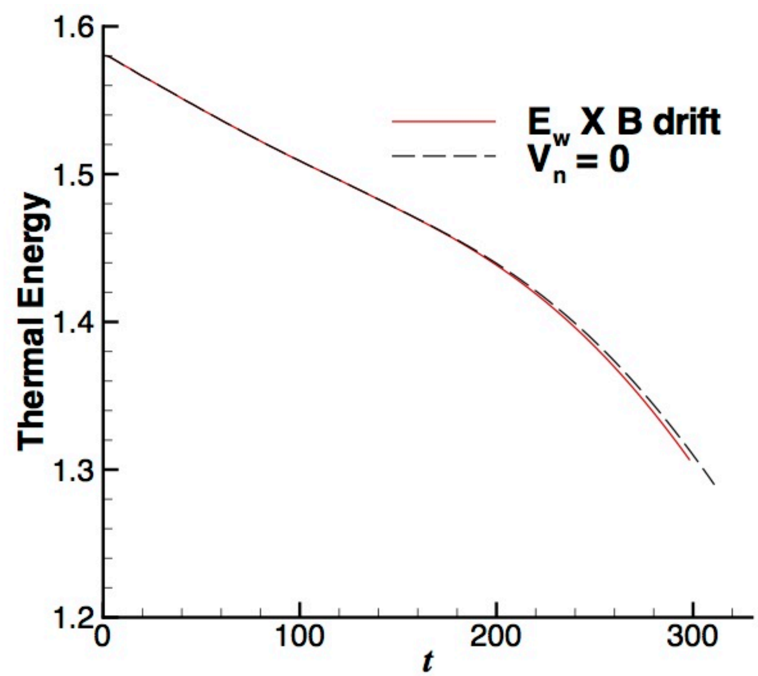

Internal energy again decays faster than current near the end of this period.

Accumulation of mass along the surface is larger with the advective mass flux condition, however.

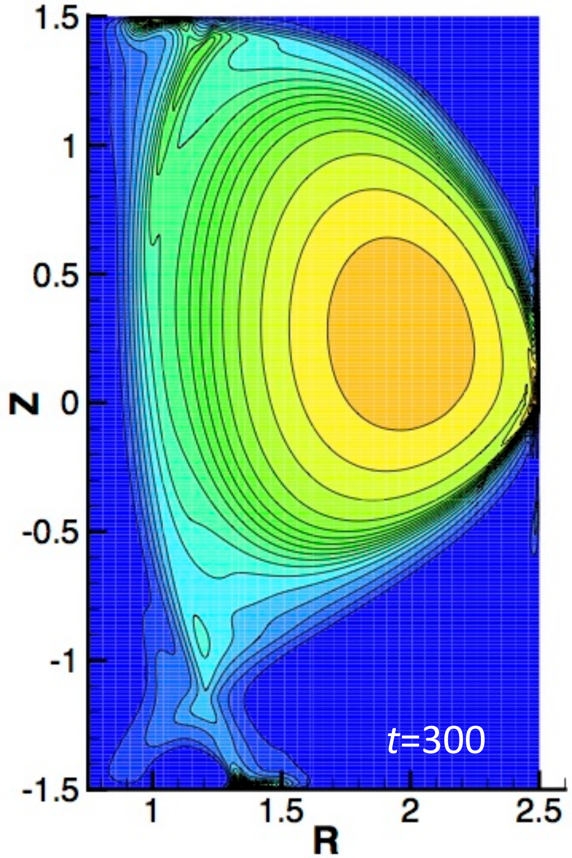

Mass density at 300 τ_A with V_n=0 and diffusive particle flux along surface.

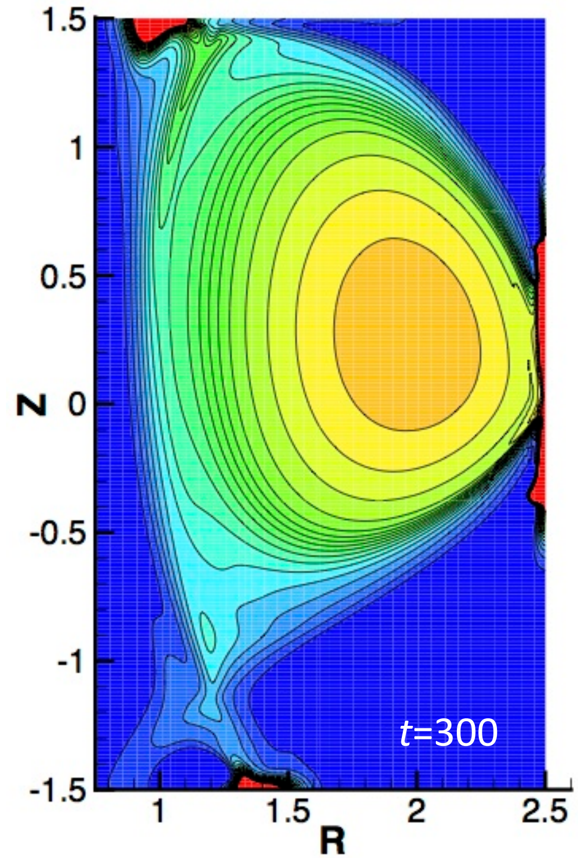

Mass density at 300 τ_A with drift outflow and advective particle flux along the surface.

The flow velocity that sends mass to the wall is larger than the $\mathbf{E}_w\times\mathbf{B}$ drift, hence the accumulation of mass.

- Along the outer wall at 300 τ_A, $\delta B\cong 0.1$ and $B_\phi=1$, so the normal component of the $\mathbf{E}_w\times\mathbf{B}$ drift is approximately 10^{-4}.
- As shown below, V_R exceeds 10^{-2}, 100 times larger, so the $\mathbf{E}_w\times\mathbf{B}$ drift is negligible.
- $B_\phi\cong 5B_{pol}$ near the outer wall, and with $V_\phi=0.07$, **V** is largely parallel to **B**.
- The magnitude of **V** is a substantial fraction of c_s (<0.25) in the edge of the simulated plasma.
- Along open field-lines, inertia is significant in the parallel force-balance.

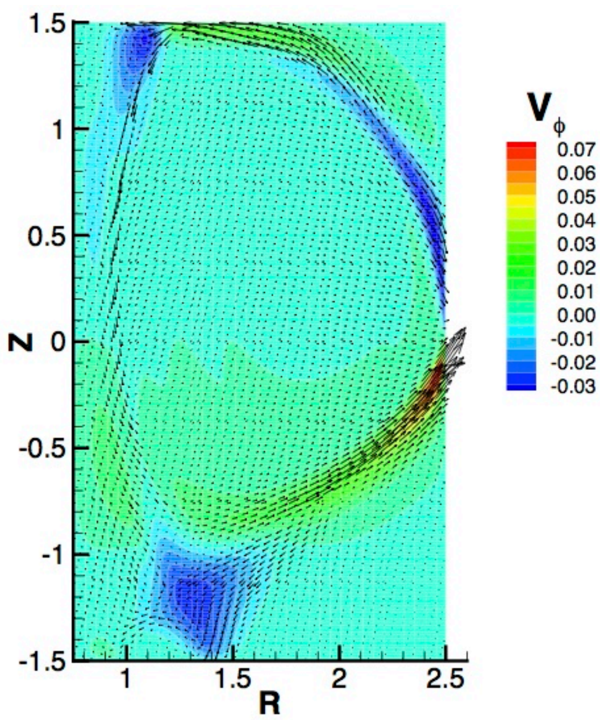

Contours of V_ϕ with poloidal vector components.

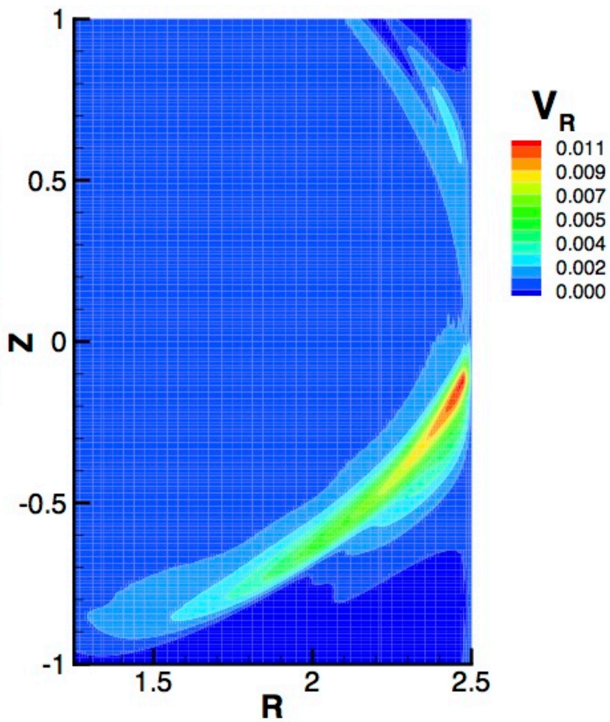

Radial component of V near contact point.

Another case does not use the outboard shaping coil, and the subsequent evolution is slower.

- The drift condition is used on V_n, but the Dirichlet condition is used for n.
- The upper limit on η is 1, and $\eta(T)$ varies by 10^6 over the central region.
- This computation uses larger numerical time-steps of ~1.7 τ_A on average.

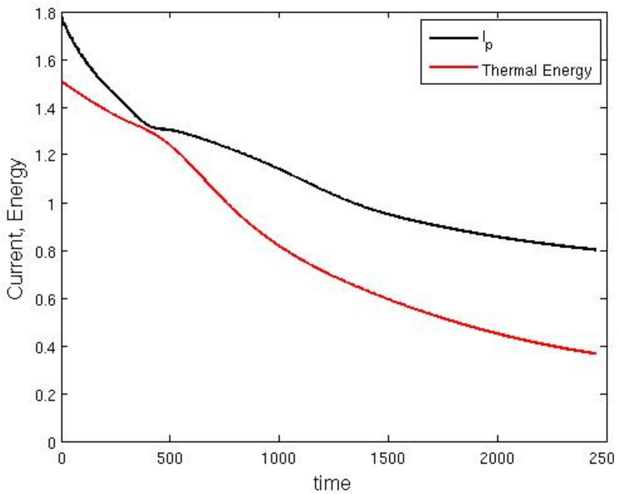

Evolution is slower than cases with the shaping coil. I_p is just below 50% after nearly 2500 τ_A.

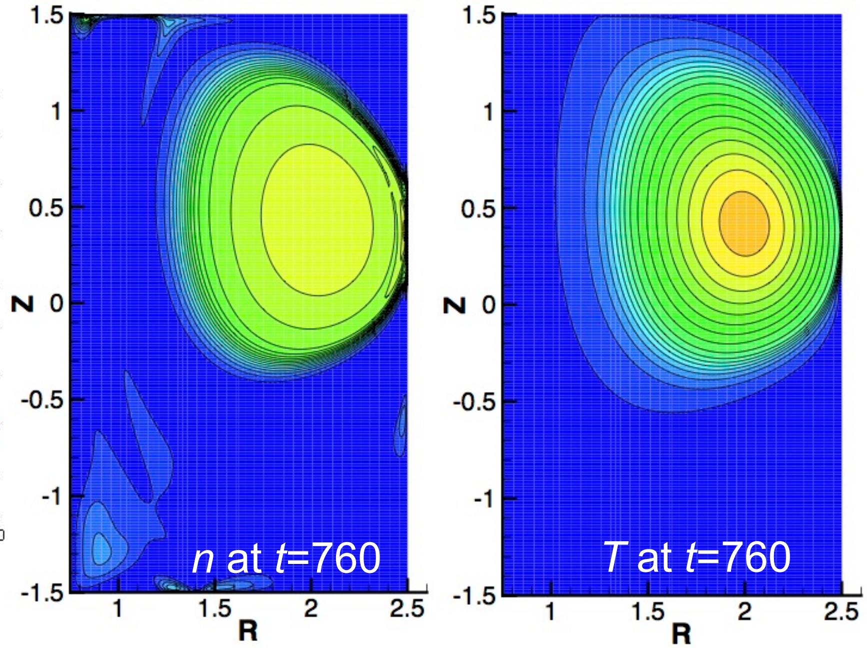

Profiles of density and temperature show greater vertical displacement.

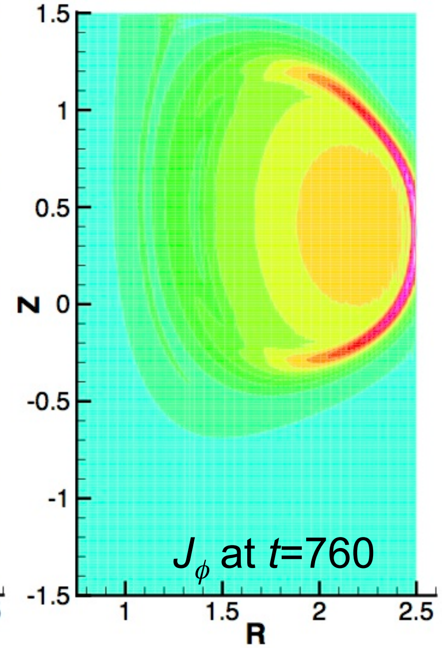

Contours of J_ϕ show a sheet of positive current.

- A reversed current sheet forms near the top in the previous case.

Discussion and Conclusions

- Development for initializing diverted tokamak equilibria with arbitrary meshing facilitates our VDE computations.
- Computations with the numerical external vacuum demonstrate representative evolution over the time-scale of the resistive wall.
- Results with $\mathbf{E}_w \times \mathbf{B}$ drift conditions at the wall and advective particle flux are similar to results with V_n=0 and Dirichlet conditions on n.
    - The extent of mass accumulation differs, however, and the diffusive-flux case allows greater loss of mass.
    - Nearly sonic parallel flows result from parallel forces.
- The need for more realistic plasma-surface modeling is evident.

Next Steps

- Resolve the discrepancy between parallel and serial calculations.
- Further develop NIMEQ for free-boundary initialization to provide more realistic VDE evolution.
- Mesh annular external regions that surround the central region.
- Apply *T*-dependent thermal conductivity and viscosity modeling.
- Implement boundary relations that model sheath conditions.
- Develop postprocessing to calculate stresses on the wall.
- Investigate coupled VDE/kink dynamics in three dimensions.

Extra Slides

For other applications, the open-field capability can be used to refine equilibria read from other solvers.

- Externally generated equilibria are interpolated to a flux-aligned mesh using the FLUXGRID code from Glasser/Kruger.
- NIMEQ re-solves the equilibrium on that mesh.

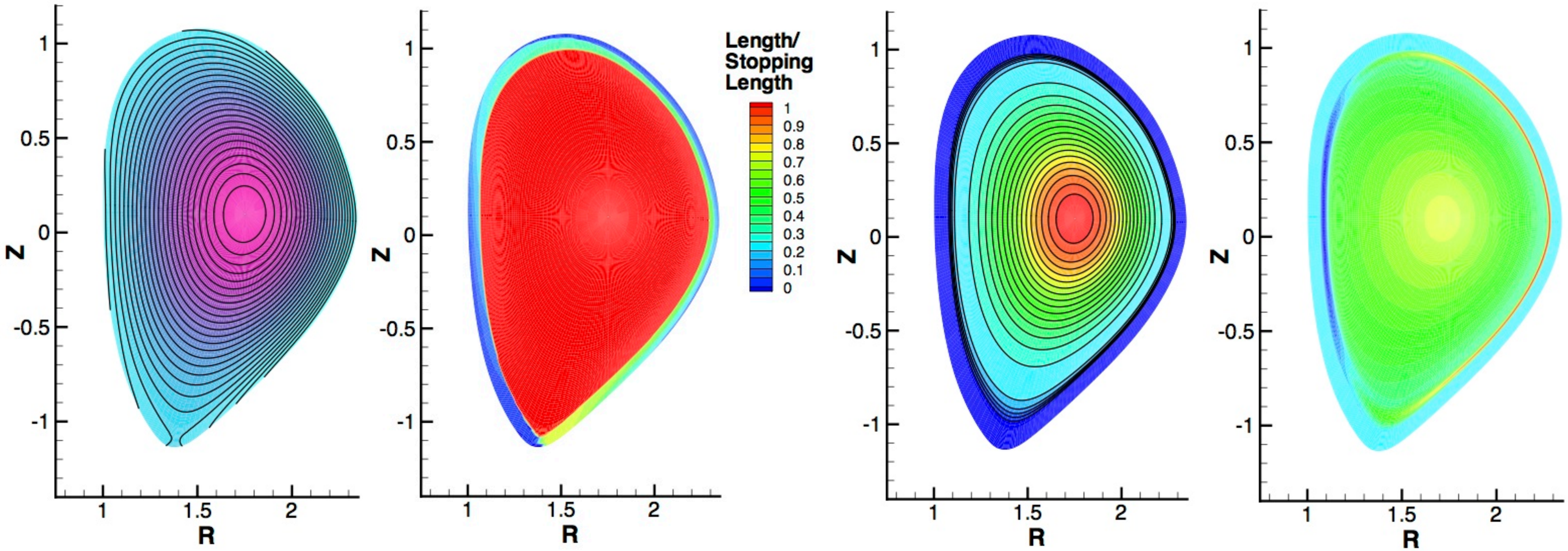

This ψ distribution is a refinement of EFIT.

Approximately aligned mesh aids B_{pol} tracing.

Pressure (left) and J_{ϕ} (right) show *H*-mode pedestal.

- A more sophisticated approach couples FLUXGRID and NIMEQ, traces the separatrix, and refines both equilibrium & mesh [King, BAPS **59**, 15, BP8.5].

Computations in the outer vacuum regions approximate magnetostatic responses.

- The standard approach uses a magnetic potential.

$$\mathbf{B} = \nabla\chi, \quad \nabla^2\chi = 0 \text{ in } R_{out}, \quad \hat{\mathbf{n}}\cdot\nabla\chi = B_{n_{out}} \text{ on } \partial R_{out}$$

where χ may be multi-valued in regions that are not topologically spherical.

- A given static solution can also be found as the long-time response to a diffusion problem.

$$\frac{\partial}{\partial t}\mathbf{B} = \eta_{out}\nabla^2\mathbf{B} \quad \text{subject to} \quad \hat{\mathbf{n}}\cdot\mathbf{B} = B_{n_{out}} \text{ on } \partial R_{out}.$$

  - This is convenient in NIMROD, which solves the plasma response in terms of **B**.
  - Induction from changes in I_p appear through surface-$\mathbf{E}_{tang}$.
  - Outer-region computations are fast relative to the plasma update.